Periodica Polytechnica Chemical Engineering, 66(3), pp. 482–493, 2022

Kinetic Model Development of the Oligomerization of High Olefin Containing Hydrocarbon By-products to Clean Engine Fuels on Amberlyst Catalyst

Ágnes Bárkányi[1*], Tamás Varga[1], Jenő Hancsók[2]

[1] Department of Process Engineering, Faculty of Engineering, University of Pannonia, Egyetem u. 10., H-8200 Veszprém, Hungary
[2] Department of MOL Hydrocarbon and Coal Processing, Faculty of Engineering, University of Pannonia, Egyetem u. 10., H-8200 Veszprém, Hungary
[*] Corresponding author, e-mail: barkanyia@fmt.uni-pannon.hu

Received: 02 December 2021, Accepted: 30 March 2022, Published online: 12 May 2022

Abstract

Nowadays, since the demand for engine fuels is continuously changing, in petroleum refineries, increasing the flexibility of gasoline/middle distillate is still an important issue, e.g. by oligomerizing light olefins (3–6 carbon atoms). The aim of our work was to develop a valid kinetic model based on the extended Eley-Rideal mechanism to describe the oligomerization of the olefin content of light naphtha by fluidized catalytic cracking (FCC) on an ion-exchange resin. Experiments were carried out in a fixed-bed tubular reactor at temperatures of between 80 and 130 °C with liquid hourly space velocities (LHSV) of between 0.5 and 2.0 1/h using Amberlyst® 15 as a catalyst. The oligomerization process was characterized based on the composition of products determined by gas chromatography. The conversion of olefins and the selectivity of the oligomerization reactions forming $C_{8\text{-}11}$ and C_{12+} hydrocarbons ($C_{8\text{-}11}$ and C_{12+} selectivity; unit: relative %) were dependent on factors that determine the reactor performance in order to identify the kinetic model parameters. Given that the developed reactor model described the measured data reasonably accurately, it can be used in terms of the optimal design of an industrial oligomerization reactor.

Keywords

olefin oligomerization, ion-exchange resin catalyst, lumped kinetic model, Eley-Rideal mechanism, determination of reaction kinetics

1 Introduction

The requirements of engine fuels are becoming stricter, making it necessary to find new technological solutions to increase the quality of these products [1]. One of the advantages of modern petroleum refineries is the existence of flexible gasoline/middle distillates, which allow them to adapt quickly to the market needs [2]. The oligomerization of light olefins and further hydrogenation (if necessary) is a possible technical solution to produce clean engine fuels. Hydrocarbons with high hydrogen contents, which burn excellently and possess other outstanding properties, can be produced [3, 4]. Furthermore, olefins that consist of various numbers of carbon atoms are important feedstocks for numerous high-value synthetic organic compounds, e.g. synthetic base oils, alcohols, detergents, etc., which are produced by oligomerization. Oligomerization of light olefins such as ethene, propene and butenes in fuels and chemicals has been a subject of research for many years [5]. Silva et al. [6] is developed design of experiments and response surface methodology models for the oligomerization of 1-butene, which allowed to study the individual and cross effects of pressure, temperature and space velocity on conversion and yields of individual product fractions. Also the oligomerization of pure 1-butene on HZSM catalyst was investigated by Díaz et al. [7] and the deactivation of the catalyst was investigated.

During oligomerization the monomers are converted to oligomer complexes to a finite degree of polymerization. An oligomer is defined as a complex molecule that is synthesized from a few monomer units. For example, dimers, trimers and tetramers are oligomers with two, three or four linking monomers, respectively [8]. Oligomerization is used in industry to produce heavier and more valuable liquid products from lighter hydrocarbon by-products with high $C_{3\text{-}6}$ olefin content. Depending on the degree of oligomerization, the products are iso-olefin-rich hydrocarbon fractions within the boiling point range of gasoline and

Cite this article as: Bárkányi, Á., Varga, T., Hancsók, J. "Kinetic Model Development of the Oligomerization of High Olefin Containing Hydrocarbon By-products to Clean Engine Fuels on Amberlyst Catalyst", Periodica Polytechnica Chemical Engineering, 66(3), pp. 482–493, 2022. https://doi.org/10.3311/PPch.19628

jet or gas oil [9]. The most important characteristic of a feedstock of oligomerization is high olefin content which can be produced by various refining and petrochemical technologies as well as almost every industrial hydrocarbon process. Light cracked naphtha (LCN) is one of the side products produced in FCC units in an industrial refinery [8]. LCN is comprised of many unsaturated alkenes such as butene (C_4), pentene (C_5) and hexene (C_6) [10].

In a really detailed review by Nicholas [5], acid and metal-catalyzed oligomerization, metallacycle mecha-nisms, multifunctional metal and acid-catalyzed oligomerization as well as some combined processes are presented for the oligomerization of light olefins to produce fuels and chemicals. In the case of light olefins (C_{2-5}), oligomerization by fuel acidic catalysts has been applied for many years. The main difference between the presented acid catalysts is their stability at higher temperatures. The application of ion-exchange resins as catalysts can yield a good degree of selectivity as far as the oligomerization of primary products is concerned, with traces of only a small number of undesired compounds being detected by gas chromatography (GC), unlike solid phosphoric acid and most zeolite catalysts, which yield multiple products from concomitant oligomerization, back-cracking and isomerization. For ion-exchange resins, the processes mentioned above are not common [11]. Ion-exchange resins have been successfully applied at low temperatures (0–100 °C) to oligomerize light olefins selectively [12, 13]. Antunes et al. [14] presented in detail the application of ion-exchange resins in the oligomerization of light olefins. It was found that cation-exchange resins have environmental and economic advantages when compared to homogeneous acid catalysts. The main disadvantages of applying resins as catalysts are their low thermal stability and irreversible deactivation at temperatures in excess of 150 °C [9].

The process of oligomerizing olefins involves a large number of hydrocarbons, thereby leading to a complex reaction network. Therefore, the kinetic modeling of this reaction network could be really complicated. As a result, different approaches to kinetic models were developed to reduce the number of equations to be solved. The kinetic models that have been presented in previous papers can be divided into two groups, namely pseudo-components or lumped and single-event kinetic models. The essence of the lumped kinetic model is that in the reaction network, the components with similar properties (but different molecular formulae and structures) are put in a hypothetical component referred to as a lumped group. The kinetic model of Ying et al. [15] is based on a number of pseudo-components concerning the interconversion of C_{2-7} olefins involving their oligomerization, cracking and aromatization. The defined lumps were: C_2; C_3; C_4; C_5; C_6; C_{7+} (including C_7 and C_8 olefins) and the Rest (aromatics and paraffins) [15]. The oligomerization of C_{3-7} olefins was described by a kinetic model consisting of pseudo-components by Huang et al. [16]. According to the respective numbers of carbon atoms, the isomers of $C_{4=}$–$C_{7=}$ were lumped together to decrease the complexity of the kinetic model [16]. The detailed kinetics of oligomerization over a commonly used commercial cation-exchange resin, Amberlyst® 15, as a catalyst was investigated [17]. A simplified lumped kinetic model based on the Langmuir-Hinshelwood-Hougen-Watson mechanism was proposed based on experiments performed in an autoclave using reactants with a purity of over 98%. A structure-oriented lumping model is presented by Quann and Jaffe [18] for describing the composition, reactions and properties of complex mixtures of hydrocarbons. Shahrouzi et al. [19] and Guillaume [20] noted that the typical lumping criteria (species-based and reaction-based generation) are insufficient to describe the reaction network of olefin oligomerization. The single-event kinetic model overcomes the drawback of the lumped kinetic models because it starts from a reaction scheme consisting of true elementary steps and uses clear physical meanings for the estimated parameters. This approach was applied successfully for modeling the oligomerization of ethylene [21]. The kinetics of the oligomerization and aromatization of ethylene over ZSM-5 has been modeled [22].

For bimolecular gas- and liquid-phase reactions, two generally used mechanisms to explain reaction kinetics are the Langmuir-Hinshelwood and Eley-Rideal mechanisms. The kinetics of the liquid-phase dimerization of isobutene in the presence of a macroporous acidic resin has been studied by Izquierdo et al. [23]. The best rate model is a two-phase semi empirical one which implies the coexistence of a Langmuir-Hinshelwood-Hougen-Watson mechanism and a modified Eley-Rideal one.

The Langmuir-Hinshelwood mechanism was applied to develop the kinetic model for the conversion of methanol to propylene over a HZSM-5 catalyst in the presence of the co-reaction of a mixture of methanol and C_{4-5} olefin [24]. The model was established using a comprehensive mechanism including the conversion of methanol, methylation, cracking, hydrogenation, dehydrogenation and oligomerization. A differential evolution algorithm was applied to

identify model parameters at different temperatures for each weight hourly space velocity (WHSV). A moderate model error can be noticed at different WHSVs, especially at lower temperatures. The oligomerization of ethylene in FCC dry gas over a HZSM-5 catalyst was studied by Ding et al. [25]. It was concluded that the dimerization of ethylene proceeded via the Eley-Rideal mechanism, while the hydrogen transfer reaction of C_3 and C_4 olefins followed the Langmuir-Hinshelwood mechanism. The effect of macroreticular acidic ion-exchange resins on the oligomerization of a mixture of 2-methyl-1-butene and 2-methyl-2-butene has been studied by Granollers et al. [26]. A heterogeneous Eley-Rideal kinetic model yielded a better fit of dimerization rates than two pseudo-homogeneous models. Gee and Williams [27] investigated the acid-catalyzed dimerization of C_8 to form C_{24} linear alpha olefins over Amberlyst® 15. Dimerization exhibited first-order kinetics in terms of both the monomer as well as catalyst and occurred via an Eley–Rideal mechanism in which the adsorbed monomer reacted with an olefin in the bulk phase.

Most of the aforementioned studies were used to model mixtures with high-purity reactants in terms of oligomerization. The aim of our work was to develop a kinetic model of the oligomerization process of a real industrial feedstock. All the unknown model parameters were identified and validated against measurements performed in a high-pressure, continuous-flow, laboratory-scale reactor system. The main expectation from the proposed kinetic model is that it can be applied in tasks concerning process optimization to determine the optimal operating conditions.

In Section 2, the experimental setup will be presented, while in Section 3, the steps of modeling will be described in detail, along with the proposed reaction mechanism, applied model equations and the used objective function. In Section 4, the experimental and simulation results will be compared and analyzed before our conclusions, results and plans for future research are presented in Section 5.

2 Experimental setup

The experiments were carried out with the light component of the full FCC distilled naphtha fraction (density at 15.6 °C: 656.1 kg/m^3, boiling point range: 30.6–88.0 °C). The composition of the investigated feedstock and other important characteristics are presented in Table 1.

The experimental works are described in detail by Kriván et al. [9]. In this paper, only a summary is presented. The schematic diagram of the applied high-pressure, continuous-flow laboratory-scale heterocatalytic reactor system can be seen in Fig. 1. The length of the fixed bed reactor is 480 mm and its internal diameter is 25 mm. In order to ensure a near to uniform temperature throughout and an even distribution of raw materials, an inert charge was placed into the bottom and top of the reactor. The effective reactor volume is approximately 100 cm^3.

Table 1 The composition and other important properties of the light FCC naphtha feedstock

Hydrocarbons	Composition, wt%
C_4 hydrocarbon	0.7
n-pentane	4.6
isopentane	36.2
C_5-olefins	24.6
cyclopentane	0.6
n-hexane	1.2
isomers of hexane	15.9
C_6-olefins	8.0
C_6-naphthenes	2.6
benzene	1.2
C_7 and heavier hydrocarbons	4.4
Total olefin content	34.2
Density (15.6 °C), kg/m^3	656.1
Engler distillation, °C	
Initial boiling point	30.6
50 %v/v	42.8
Final boiling point	88.0

The oligomerization experiments were carried out over Amberlyst® 15, which is an ion-exchange-type acidic catalyst. Table 2 contains the properties of the applied catalyst. Given that it is a continuous system with a reactor with a catalyst charge of 80 cm^3, the catalyst was not changed after each experiment. The experiments were performed

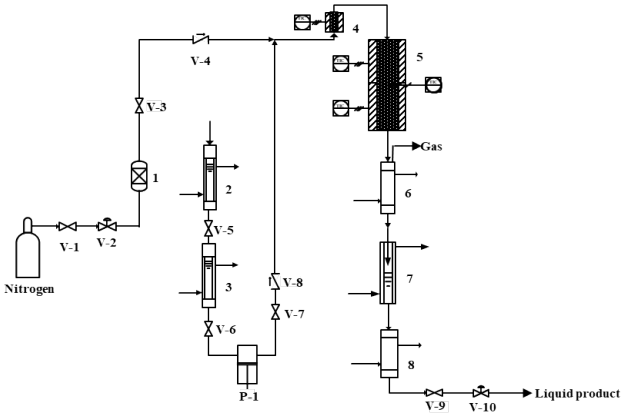

Fig. 1 Simplified scheme of the experimental reactor system (based on [9]): 1) gas filter; 2), 3) burettes for liquid feed; 4) pre-heater; 5) reactor; 6), 8) cooler; 7) separator; V-1, V-3, V-5, V-6, V-7, V-9 closing valves; V-2, V-10 control valve; V-4, V-8 back valve; P-1 pump)

Table 2 Main properties of the ion-exchange catalyst (based on [9])

Properties	Catalyst
Concentration of active sites, eq/kg	4.78
Water content, %	<1.6
Surface area, m^2/g	51
Average pore diameter, nm	30.4
Pore volume, cm^3/g	0.38

in series at a given liquid hourly space velocity (LHSV), starting with the lowest temperature. The samples were extracted once all the measured state variables had stabilized (i.e. once the system had reached its steady state). No evidence to suggest that the catalyst had become deactivated was found during the experiments. In contrast, above 110 °C the deactivation of catalyst can be experienced.

The investigated temperature range was 80–130 °C at a pressure of 30 bar and the LHSV range was 0.5–3.0 1/h. At higher temperatures (over 150 °C based on [14]), in line with recommendations from the manufacturers of ion-exchange resins, no experiments were carried out to avoid significant thermal degradation of the resin [9]. The liquid yield was quantified by mass measurements. The composition of the liquid hydrocarbon products was characterized by a gas chromatographer equipped with a FID (Flame Ionization Detector) and SPB-1 (30 m × 0.25 mm × 0.25 µm) or Chrompack CP7515 (50 m × 0.32 mm × 5 µm) column. The chromatographic peaks were assigned by GC–MS (Gas Chromatography–Mass Spectrometry) measurements (Shimadzu GC-2010 Plus gas chromatograph, Shimadzu GCMS-QP2010 SE mass spectrometer). The equipment was calibrated with hydrocarbon mixtures of known compositions. To calculate the olefin conversion ratio, the olefin content of the feedstock and the unconverted C_{4-6} olefins in the liquid product could be determined. Proper, detailed component analysis of the products was not performed; the heavier components in the liquid product compared to the unconverted components of the raw material were considered as the reaction product. The results were evaluated by dividing the C_{8+} products into two fractions based on carbon number, thereby giving the C_{8-11} (Eq. (1)) to C_{12+} (Eq. (2)) ratio (S) in the C_{8+} product [9].

$$S_{C_{8-11}} = \frac{m_{C_{8-11}}}{m_{C_{8+}}} \times 100\% \tag{1}$$

$$S_{C_{12^+}} = 100\% - S_{C_{8-11}} \tag{2}$$

3 Developed model

Based on the literature review, the Eley-Rideal kinetic model combined with the rate equations of adsorption and desorption is considered to develop the reactor model. As is shown in Table 1, the amounts of C_4 and C_7 olefins were negligible compared to those of C_5 and C_6 olefins in the investigated feedstock. Therefore, during the modeling, only the C_5 and C_6 olefins were taken into consideration. The proposed reaction mechanism, applied model equations and the applied objective function will be presented in detail in the following sections.

3.1 The proposed reaction mechanism

Fig. 2 demonstrates the scheme of the applied kinetic mechanism. C_i^* denotes each adsorbed component (olefins and oligomers) in the catalyst, while C_i denotes each component (olefins and oligomers) in the fluid phase.

During the modeling, 14 process steps were taken into consideration (Table 3). The first ten steps are actually the adsorption (IDs. R1, R3, R5, R7 and R9) and desorption

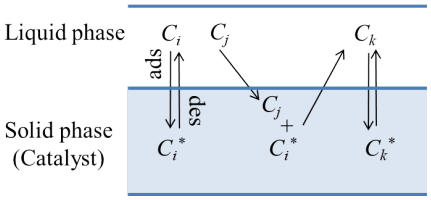

Fig. 2 Simplified schematic diagram of the considered reaction system (the *i* and *j* subscripts denote the olefin components, while the *k* subscript denotes the oligomer component)

Table 3 List of the considered process steps of the oligomerization of C_{5-6} olefins

Process step/Reaction	ID
$C_5 + Cat \underset{k_2}{\overset{k_1}{\rightleftharpoons}} C_5^*$	R1 R2
$C_6 + Cat \underset{k_4}{\overset{k_3}{\rightleftharpoons}} C_6^*$	R3 R4
$C_{10} + Cat \underset{k_6}{\overset{k_5}{\rightleftharpoons}} C_{10}^*$	R5 R6
$C_{11} + Cat \underset{k_8}{\overset{k_7}{\rightleftharpoons}} C_{11}^*$	R7 R8
$C_{12} + Cat \underset{k_{10}}{\overset{k_9}{\rightleftharpoons}} C_{12}^*$	R9 R10
$C_5^* + C_5 \xrightarrow{k_{11}} C_{10} + Cat$	R11
$C_6^* + C_6 \xrightarrow{k_{12}} C_{12} + Cat$	R12
$C_5^* + C_6 \xrightarrow{k_{13}} C_{11} + Cat$	R13
$C_6^* + C_5 \xrightarrow{k_{14}} C_{11} + Cat$	R14

(IDs. R2, R4, R6, R8 and R10) of the considered components. The last four steps (IDs. R11-R14) are the oligomerization reactions.

3.2 Applied model equations

For modeling purposes, the two phases present in the tubular reactor must be treated quasi-independently. The steady-state plug flow model was used to model the moving liquid phase. Nevertheless, the fixed, solid catalytic bed was described with a quasi-stationary model. This was necessary because the concentration of active sites on the catalyst should be continuously calculated.

The balanced equation for the components in the fluid phase is the following:

$$\frac{dB_i}{dx} = V_{\text{catalyst}} \times R_{C_i}, \tag{3}$$

where i defines the components such as C_5 and C_6 olefins as well as the oligomers, B denotes the molar flow rate of the input (mol/h), x represents the dimensionless length of the catalyst bed, V_{catalyst} stands for the volume of the catalyst (cm^3) and R_{C_i} refers to the source of the i-th component ($mol/cm^3/h$). The following molecular weights were applied in simulations in the case of olefins ($C_{5\text{-}6}$) and oligomers ($C_{10\text{-}12}$): 70, 84, 140, 154 and 168 g/mol, respectively.

The rates of the considered processes are shown in Table 3 IDs. R1-R10 and are given by Eqs. (4)–(6), where the reaction order is regarded as proportional to the stoichiometric coefficient. In Eq. (4)–(6), i denotes the olefins and oligomers too, but j only represents the olefins. It should be noted that i and j can be equal.

Adsorption of components:

$$r_a = [C_i] \times [Cat] \times k_a, \quad a = 1,3,5,7,9. \tag{4}$$

Desorption of components:

$$r_d = [C_i^*] \times k_d, \quad d = 2,4,6,8,10. \tag{5}$$

Oligomerization reactions due to the mechanism:

$$r_o = [C_i^*] \times [C_j] \times k_o, \quad o = 11,12,13,14. \tag{6}$$

Then the rate of formation of each component (R_{C_i}) can be obtained based on the following stoichiometric matrix (Table 4).

The amounts of adsorbed components were calculated using a quasi-stationary model. Accordingly, the concentration of the adsorbed components can be calculated by Eqs. (7)–(11):

$$[C_5^*] = \frac{k_1 \times [C_5] \times [Cat]}{k_2 + k_{11} \times [C_5] + k_{13} \times [C_6]} \tag{7}$$

$$[C_6^*] = \frac{k_3 \times [C_6] \times [Cat]}{k_4 + k_{12} \times [C_6] + k_{14} \times [C_5]} \tag{8}$$

$$[C_{10}^*] = \frac{k_5 \times [C_{10}] \times [Cat]}{k_6} \tag{9}$$

$$[C_{11}^*] = \frac{k_7 \times [C_{11}] \times [Cat]}{k_8} \tag{10}$$

$$[C_{12}^*] = \frac{k_9 \times [C_{12}] \times [Cat]}{k_{10}}. \tag{11}$$

Table 4 Stoichiometric matrix of the considered processes (−1: the component is consumed in the reaction; 1: the component is formed in the reaction)

Components \ Reactions	r_1	r_2	r_3	r_4	r_5	r_6	r_7	r_8	r_9	r_{10}	r_{11}	r_{12}	r_{13}	r_{14}
C_5	−1	1									−1			−1
C_6			−1	1								−1	−1	
C_{10}					−1	1					1			
C_{11}							−1	1					1	
C_{12}									−1	1		1		
C_5^*	1	−1									−1		−1	
C_6^*			1	−1								−1		−1
C_{10}^*					1	−1								
C_{11}^*							1	−1						
C_{12}^*									1	−1				
Cat	−1	1	−1	1	−1	1	−1	1	−1	1	1	1	1	1

The concentration of unoccupied catalytic active sites can be calculated by Eq. (12):

$$[Cat] = [Cat_{sum}] - [C_5^*] - [C_6^*] - [C_{10}^*] - [C_{11}^*] - [C_{12}^*], \quad (12)$$

where $[Cat_{sum}]$ denotes the total concentration of catalytic active sites. The temperature dependencies of the overall kinetic constants (k_o) of the oligomerization reactions were described by Arrhenius-type equations:

$$k_o = A_o \times \exp\left(\frac{-E_{A_o}}{R \times T}\right), \quad o = 11,12,13,14. \quad (13)$$

Furthermore, the temperature dependencies of the adsorption and desorption rate constants were defined on the basis of the Van't Hoff equation:

$$k_{da} = A_{da} \times \exp\left(\frac{-\Delta H_{da}}{R \times T}\right), \quad da = 1,2,\ldots,10. \quad (14)$$

The experiments demonstrated that catalyst activation decreased significantly as the temperature rose. The following formula was used to account this phenomenon in our case:

$$[Cat_{sum}] = a \times \left(1 - \frac{\left(\tanh\left(\frac{T^*}{b}\right)+1\right)}{2}\right). \quad (15)$$

Parameter a yields the total amount of catalytic active sites, while b determines the rate of catalyst deactivation as a function of temperature. The $\left(1 - \frac{\left(\tanh\left(\frac{T^*}{b}\right)+1\right)}{2}\right)$ term will be more or less equal to 1 if $T^* < -3$ and practically 0 if $T^* > 3$ when $b = 1$. Based on our results, it was our aim to demonstrate that the catalytic activity starts to decrease above 110 °C. Therefore, it would be desirable for the catalytic activity to be at its maximum at four temperatures, namely 80, 90, 100 and 110 °C. Consequently, the range below −3 was arbitrarily increased so that the maximum activity would be exhibited at those four temperatures. Accordingly, the range of T^* was defined as [−15:3]. Therefore, T = 80 °C corresponds to T^* = −15 and T = 130 °C corresponds to T^* = 3. During the simulations, the following formula was used to calculate the required T^* from the given temperatures at which the experiment was conducted:

$$T^* = \frac{T - T_{\min}}{T_{\max} - T_{\min}} \times 18 - 15. \quad (16)$$

Fig. 3 represents the final shape of the abovementioned deactivation function in the desired temperature range, when b = 1.

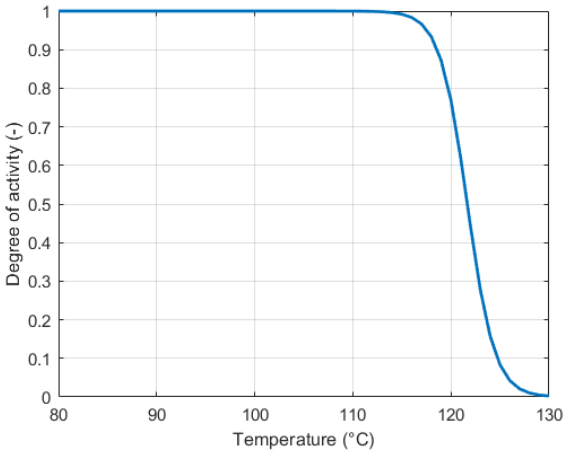

Fig. 3 The shape of the deactivation function $\left(1 - \frac{\left(\tanh\left(\frac{T^*}{b}\right)+1\right)}{2}\right)$ when b = 1

The pre-exponential factors (A_o, A_{da}), the activation energy (E_{A_o}), the heat of sorption (ΔH_{da}) as well as the parameters a and b were the 30 unknown model parameters that should be identified based on the experimental data.

3.3 Applied objective function

The introduced model equations were solved in MATLAB R2019a using the Runge−Kutta method. Since the reaction rate constants were identified simultaneously at all temperatures (T = 80, 90, 100, 110, 120 and 130 °C), the objective function was the normalized absolute error between the calculated and measured data for olefin conversion and C_{12+} selectivity at all temperatures and at each LHSV:

$$\text{Objective function} = \sum_T \left(\frac{\left|\left(S_T^{exp} - S_T^{cal}\right)\right|}{S_T^{exp}} + \frac{\left|\left(X_T^{exp} - X_T^{cal}\right)\right|}{X_T^{exp}} \right), \quad (17)$$

where S_T^{exp} and X_T^{exp} denote the experimental C_{12+} selectivity and olefin conversion rate at temperature T, respectively, while S_T^{cal} and X_T^{cal} represent the calculated C_{12+} selectivity and olefin conversion rate at temperature T, respectively.

The MATLAB built-in genetic algorithm was applied to determine the minimum of the objective functions at different LHSVs. The population size was 3,000 and the default mutation function, Gaussian type, was applied to identify the parameters.

4 Results and discussion

In this section, the experimental and simulation results obtained will be introduced and discussed in detail.

4.1 Experimental results

Oligomerization reactions are exothermic, so the temperature increase is favorable within the kinetic range. Nevertheless, at a high temperature (350 °C based on [28]), thermodynamic inhibition becomes significant [24]. Furthermore, based on the experimental results of Ying et al. [15], during the oligomerization, the probability of two dimer molecules joining together is less than that of a dimer with a monomer, followed by the subsequent trimer joining to another monomer. The lower concentration and poorer mobility of dimers compared to monomers might explain the aforementioned phenomena. Above 110–120 °C, the activity of some ion-exchange resins decreases because of two main reasons; on the one hand, the resin loses some of its sulfonic acid functional groups but on the other hand, the formation of oligomers with high molecular weights may cover the active sites [5, 29, 30]. An increase in the LHSV favors the formation of the heavier products (C_{12+}) up to a certain limit and the desorption of molecules from the surface of the catalyst. At higher LHSVs, the C_{12+} selectivity will decrease due to the shortening of the residence time [24].

Olefin conversion and C_{12+} selectivity characterized the oligomerization reactions which took place on the catalyst. Since the yield of the liquid product was over 98% at every process parameter, the rates of the cracking reactions, which results in gas-phase hydrocarbons, were relatively small over the studied temperature range due to the relatively low experimental temperature [9].

The experimental results are shown in Fig. 4 and Fig. 5. Both the olefin conversion and C_{12+} selectivity monotonically increased within the temperature range of 80–110 °C. Above 110 °C, the conversion rate decreased because of the deactivation of the ion-exchange resin. Fig. 4 shows that the higher the LHSV is, the lower the

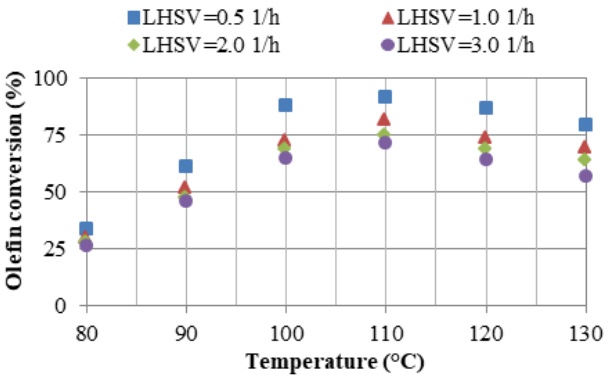

Fig. 4 Olefin conversion as a function of the reactor temperature at different LHSVs

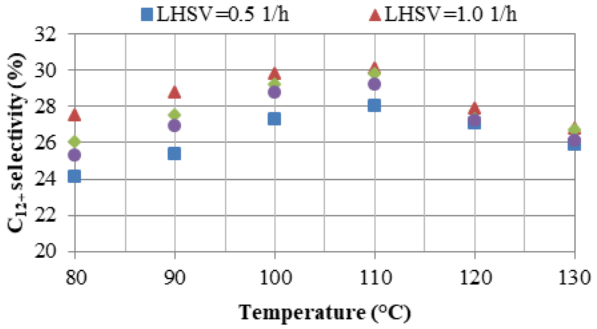

Fig. 5 C_{12+} selectivity as a function of the reactor temperature at different LHSVs

monomer conversion at every temperature. Nevertheless, in the case of C_{12+} selectivity, such a tendency is not seen with regard to the function of LHSV (Fig. 4). As can be seen in Fig. 4 and Fig. 5, the conversion and selectivity can be maximized at a specific LHSV, which means that the rate of surface regeneration of the catalyst is similar to the rate of oligomerization. It can be said that the C_{12+} selectivity is the highest and lowest at every measured temperature when LHSV = 1.0 and 0.5 1/h, respectfully. All these data are consistent with the results published by Bellussi et al. [31]. They noticed a maximum rate of olefin conversion as a function of WHSV, due to the diffusion inhibition of the catalyst HZSM-5 with regard to bulky branched olefins (shape-selectivity of products). During the investigation of how the time-on-stream affected the performance of the catalyst, they noticed pore plugging caused by the products of high molecular weights and the production of mixtures of oligomers with shorter average chain lengths.

4.2 Simulation results

As was previously mentioned, the proposed model consists of 30 unknown parameters that should be determined to create a valid reactor model. Eq. (15) describes the total concentration of active sites on the catalyst as a function of the temperature. Therefore, parameters *a* and *b* in Eq. (15) are independent of LHSV so the first step of the identification was to determine these two parameters. All 30 unknown model parameters at each LHSV (Eq. (17)) were identified separately and almost the same parameters were obtained at each LHSV. The average of the identified values of *a* and *b* was taken, moreover, in the subsequent identification steps, these values were fixed at each LHSV. The fixed parameters were $a = 10.7$ and $b = 2.3$. In this case, the total amount of active sites on the catalyst as a function of temperature can be seen in Fig. 6.

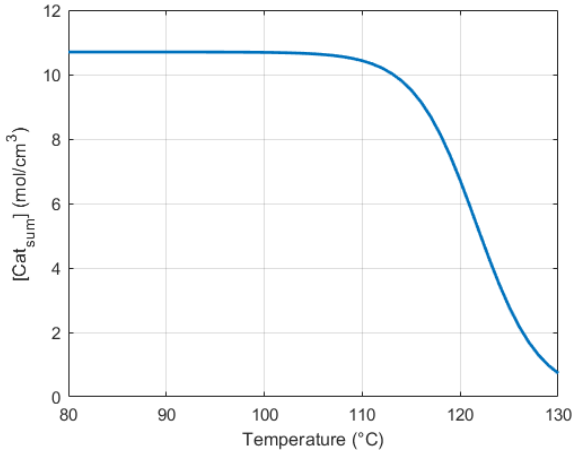

Fig. 6 The identified shape of Eq. (15), which describes the total concentration of active sites on the catalyst [Cat_{sum}] as a function of temperature (a = 10.7 and b = 2.3)

Following this, the identification procedure consisted of three steps which are presented in detail below.

Step 1: In this step, the remaining 28 unknown model parameters consisted of the pre-exponential factors (A_o, A_{da}), the activation energy (E_{A_o}) and heat of sorption (ΔH_{da}). Therefore the model parameters were tested to identify which ones accurately describe the temperature dependency of olefin conversion and C_{12+} selectivity at each LHSV. Fig. 7 (a) and (b) show two examples of the achieved model fit in this step at LHSVs of 1.0 1/h and 3.0 1/h, respectively. It can be seen that the model and experimental data fitted well at all temperatures. The values of Eq. (17) at LHSVs of 1.0 1/h and 3.0 1/h were 0.4788 and 0.681, respectively. The result of this step was four sets of kinetic parameters, one set for each LHSV.

Step 2: After the analysis of the experimental results, it was proposed that the velocity of the fluid could be affected by the activity of the catalyst due to a positive effect on the rate of surface regeneration. Hence, the identified parameters in the previous step were depicted as a function of LHSV, moreover, it was noted that second-degree polynomials could also be fitted. Two example results are shown in Fig. 8 (all of the results can be seen in the Supplement). The R^2 values are also depicted in Fig. 8 (a) and (b). These values fell within the range of 0.9–1.0. Only two parameters, namely A_6 and ΔH_5, were below 0.9. Hence, the obtained correlations between LHSV and kinetic model parameters can be applied to calculate the kinetic parameters at each LHSV.

The results of this step produced 28 equations, each of which consisted of three parameters. The form of the equations was:

$$f(\mathrm{LHSV}) = p_1 \times \mathrm{LHSV}^2 + p_2 \times \mathrm{LHSV} + p_3\,, \qquad (18)$$

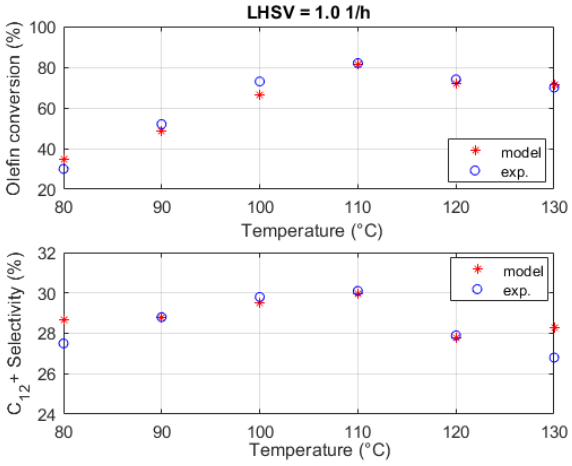

(a)

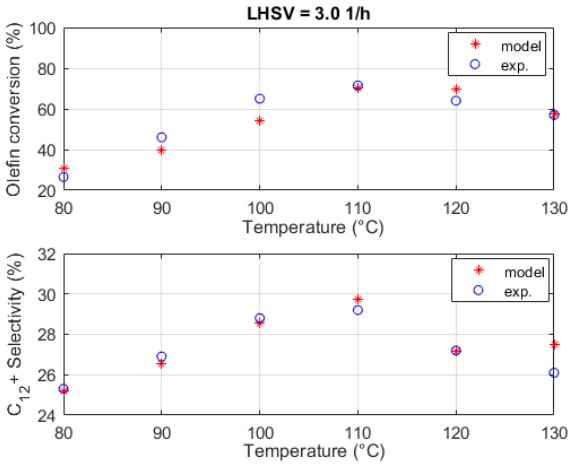

(b)

Fig. 7 The results of identification in Step 1: The change in olefin conversion (%) and C_{12+} selectivity (%) as a function of temperature ((a) LHSV = 1.0 1/h, Obj. fun. = 0.4788; (b) LHSV = 3.0 1/h, Obj. fun. = 0.681; o: experimental results, *: simulation results)

where f(LHSV) denotes the kinetic parameter and p_1, p_2 as well as p_3 represent the coefficients of the fitted second-degree polynomials. Using these equations, the required kinetic parameters can be determined for any LHSV within the given range. The coefficients of the fitted second-degree polynomials for each kinetic parameter with 95% confidence bounds are presented in Table 5.

Step 3: The sets of kinetic parameters at each LHSV were calculated based on the equation identified in the previous step. Validation of the model took into account the estimated parameters at each LHSV as the last step of the identification procedure. The results in the case of LHSV = 1.0 1/h as an example are presented in Fig. 9.

In this case, the value of Eq. (17) was 0.7515, which is slightly higher than in Step 1. In Fig. 9, the olefin conversion and C_{12+} selectivity at an LHSV of 1.0 1/h can be seen. It can be observed that the model performance is the

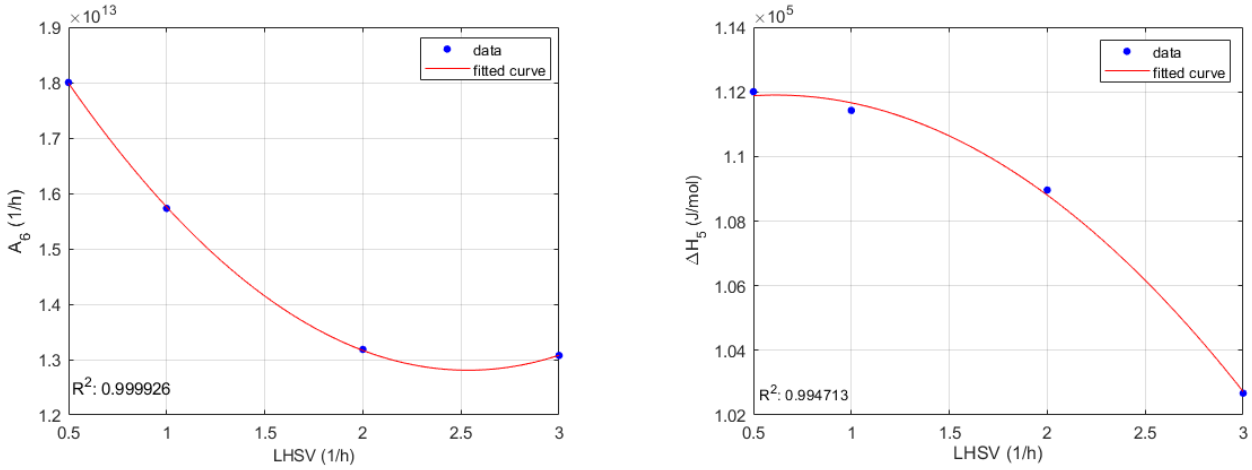

(a) (b)

Fig. 8 The results of curve fitting in Step 2: The change in the identified parameters ((a) A_6 (1/h) and (b) ΔH_5 (J/mol)) as a function of LHSV; R^2 values are indicated

Table 5 The coefficients (p_1, p_2 and p_3) of the fitted second-degree polynomials for the pre-exponential factors (cm³/mol/h or 1/h), activation energies (J/mol) and the heat of sorption (J/mol) with 95% confidence bounds

Pre-exponential factor (cm³/mol/h) or (1/h)	p_1 (Coefficient)	p_2 (Coefficient)	p_3 (Coefficient)	Activation energy (J/mol)	p_1 (Coefficient)	p_2 (Coefficient)	p_3 (Coefficient)
A_1	4.0498951×10^{12}	$-1.6241257 \times 10^{13}$	5.9003512×10^{13}	ΔH_1	4.5131502×10^{3}	-1.4655702×10^{4}	9.7221797×10^{4}
A_2	$-4.1295757 \times 10^{13}$	1.5533506×10^{14}	8.2178069×10^{13}	ΔH_2	-5.2823197×10^{3}	1.8005191×10^{4}	8.4584645×10^{4}
A_3	1.1471756×10^{18}	$-3.9007197 \times 10^{18}$	7.2035474×10^{18}	ΔH_3	1.7218318×10^{3}	-6.9428019×10^{3}	1.2099393×10^{5}
A_4	1.2099299×10^{12}	$-4.4441205 \times 10^{12}$	1.1995220×10^{13}	ΔH_4	-7.5909384×10^{3}	3.5352742×10^{4}	7.0190525×10^{4}
A_5	$-2.6936676 \times 10^{14}$	1.1295274×10^{15}	8.8110798×10^{13}	ΔH_5	-1.6125084×10^{3}	1.9810346×10^{3}	1.1129132×10^{5}
A_6	1.2512331×10^{12}	$-6.3428851 \times 10^{12}$	2.0846747×10^{13}	ΔH_6	-4.8986249×10^{2}	2.9202230×10^{3}	1.0664299×10^{5}
A_7	$-4.2586718 \times 10^{14}$	2.1311917×10^{15}	9.5880460×10^{14}	ΔH_7	-6.9761593×10^{2}	-7.1318063×10^{2}	9.2447777×10^{4}
A_8	$-1.7382094 \times 10^{11}$	5.2766866×10^{11}	7.8734695×10^{11}	ΔH_8	-1.1945064×10^{4}	4.2272527×10^{4}	8.6168508×10^{4}
A_9	$-3.8844106 \times 10^{11}$	1.7815074×10^{12}	2.5159022×10^{11}	ΔH_9	1.0429558×10^{4}	-4.2295534×10^{4}	1.2049663×10^{5}
A_{10}	$-2.9626414 \times 10^{11}$	1.1119178×10^{12}	3.4123607×10^{11}	ΔH_{10}	-5.6984785×10^{3}	2.0396577×10^{4}	8.1241513×10^{4}
A_{11}	$-2.6158814 \times 10^{17}$	5.4691030×10^{18}	3.4040289×10^{19}	$E_{A_{11}}$	-7.9389287×10^{3}	2.4992300×10^{4}	1.1574798×10^{5}
A_{12}	$-1.0138898 \times 10^{12}$	2.8840820×10^{12}	7.0651198×10^{12}	$E_{A_{12}}$	-3.6667039×10^{2}	8.2035044×10^{1}	5.1096462×10^{4}
A_{13}	2.4714556×10^{18}	$-7.4470525 \times 10^{18}$	5.3024689×10^{19}	$E_{A_{13}}$	-3.2298145×10^{3}	2.3761566×10^{4}	2.1363674×10^{5}
A_{14}	3.1383721×10^{9}	$-1.1386363 \times 10^{10}$	4.1190038×10^{10}	$E_{A_{14}}$	-7.1173347×10^{3}	3.2124595×10^{4}	4.5649949×10^{4}

lowest at 120 °C. At the other temperatures, the simulated and measured data closely fit. The achieved model performance was similar at other LHSVs as it is shown in Fig. 10. The anomaly observed at 120 °C may be due to the method of calculating the catalyst deactivation.

In Fig. 10, the correlations between the measured and simulated data (Fig. 10 (a) olefin conversion (%); Fig. 10 (b) C_{12+} selectivity (%)) are demonstrated. From Fig. 10, it can be seen that the developed model describes the experimental data with an acceptable degree of precision. The correlation with C_{12+} selectivity appears to be slightly poorer than with olefin conversion due to the fact that the range of C_{12+} selectivity values was much narrower than in the case of olefin conversion.

5 Conclusion

In this paper, a kinetic model was presented for modeling the oligomerization of a light FCC naphtha fraction over the Amberlyst® 15 ion-exchange resin. The experiments were carried out in a high-pressure, continuous-flow, laboratory-scale reactor system. The investigated temperature range was 80–130 °C, under a pressure of 30 bar and over a

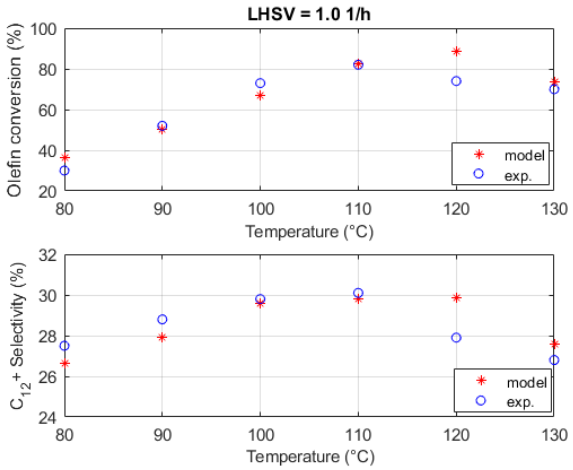

Fig. 9 The change in olefin conversion (%) and C_{12+} selectivity (%) as a function of temperature at LHSV = 1.0 1/h (o: experimental results, *: simulation results) when the kinetic parameters were calculated from the equations of the fitted second-degree polynomials, Obj. fun. = 0.7515.

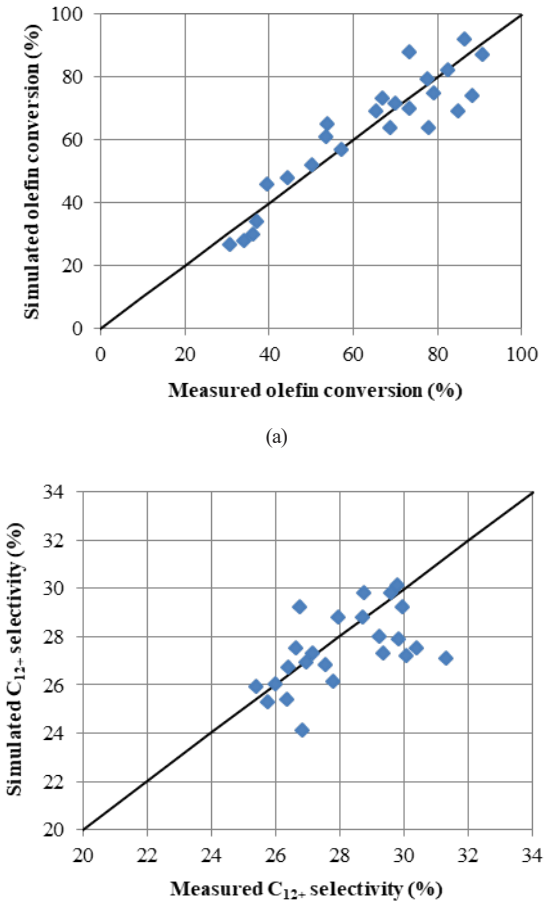

Fig. 10 Correlation between the measured and simulated data in the case of Step 3 ((a) Olefin conversion (%); (b) C_{12}^{+} selectivity (%))

LHSV range of 0.5–3.0 1/h. Monomer conversion and C_{12+} selectivity was the basis for identification. The extended Eley-Rideal mechanism was applied during the modeling. A quasi single-phase model was developed for the tubular fixed-bed reactor. The thermal deactivation of the catalyst was taken into account. The reaction network consisted of 14 process steps. The first ten steps were the adsorption and desorption of the considered components ($C_{5\text{-}6}$ olefins and $C_{10\text{-}12}$ oligomers), moreover, the last four were the oligomerization reactions. During the identification step, 30 unknown model parameters (28 kinetic parameters and 2 parameters that influence catalyst deactivation) were identified. In the first step of the identification process, the kinetic parameters at each LHSV were identified separately, resulting in four sets of kinetic parameters. In the second step, as a function of LHSV, a second-degree polynomial was fitted to all the kinetic parameters. In the third step, the equations of the fitted second-degree polynomials were applied to calculate the kinetic parameters with 95% confidence bounds.

Based on the results presented above, it can be said that the developed model is suitable to describe the oligomerization of the light part of a full FCC naphtha fraction over the ion-exchange resin Amberlyst® 15. Therefore, this model can be used to further analyse the process and optimize the process variables as well as the light FCC naphtha feedstock with other mass fractions.

Acknowledgement

We acknowledge the financial support of Széchenyi 2020 under the project GINOP-2.3.2-15-2016-00053. The contribution of Tamás Varga to this paper was supported by the János Bolyai Research Scholarship of the Hungarian Academy of Sciences. We are grateful for the work of Eszter Kriván in performing the physical measurements.

Abbreviations

A: pre-exponential factor [cm^3/mol/h or 1/h]
B: the molar flow rate of the input [mol/h]
C: unabsorbed component
C^*: adsorbed component
Cat: catalyst
$[C]$: concentration of the unadsorbed component [mol/cm^3]
$[Cat]$: concentration of active sites on the catalyst [mol/cm^3]
$[Cat_{sum}]$: total concentration of active sites on the catalyst [mol/cm^3]
E_A: Activation energy [J/mol]
R: gas constant [J/mol/K]
R_C: component source [$mol/cm^3/h$]
S: selectivity [%]
T: temperature [°C], in Eqs. (13) and (14). temperature [K]
T^*: rescaled temperature in Eq. (16) [-]

$V_{catalyst}$: catalyst volume [cm^3]
a: total amount of active sites on the catalyst in Eq. (15)
b: the speed of catalyst deactivation as a function of temperature in Eq. (15)
f(LHSV): kinetic parameter in Eq. (18)
p_1, p_2, p_3: coefficients of the fitted second-degree polynomials in Eq. (18)
k: rate coefficient [cm^3/mol/h or 1/h]
r: reaction rate [mol/cm^3/h].

Subscripts
a: adsorption, a = 1,3,5,7,9
d: desorption, d = 2,4,6,8,10
i: olefin and oligomer components, i = 5,6,10,11,12
j: olefin components, j = 5,6
k: oligomer components, k = 10,11,12
o: oligomerization, o = 11,12,13,14
exp: experimental data
model: modelled data
min: minimum
max: maximum.

References

[1] Moriarty, P., Honnery, D. "Greening passenger transport: a review", Journal of Cleaner Production, 54, pp. 14–22, 2013. https://doi.org/10.1016/j.jclepro.2013.04.008
[2] Srivastava, S. P., Hancsók, J. "Fuels and fuel-additives", Wiley, Hoboken, USA, 2014.
[3] Hancsók, J., Visnyei, O., Holló, A., Leveles, L., Thernesz, A., Varga, G., Valyon, J. "Alternative diesel fuels with high hydrogen content in their molecular structures", Renewable Energy, 142, pp. 239–248, 2019. https://doi.org/10.1016/j.renene.2019.04.105
[4] Hancsók, J., Kasza, T., Visnyei, O. "Isomerization of n-C_5/C_6 Bioparaffins to Gasoline Components with High Octane Number", Energies, 13(7), Article number: 1672, 2020. https://doi.org/10.3390/en13071672
[5] Nicholas, C. P. "Applications of light olefin oligomerization to the production of fuels and chemicals", Applied Catalysis A: General, 543, pp. 82–97, 2017. https://doi.org/10.1016/j.apcata.2017.06.011
[6] Silva, A. F., Neves, P., Rocha, S. M., Silva, C. M., Valente, A. A. "Optimization of continuous-flow heterogeneous catalytic oligomerization of 1-butene by design of experiments and response surface methodology", Fuel, 259,Article number: 116256, 2020. https://doi.org/10.1016/j.fuel.2019.116256
[7] Díaz, M., Epelde, E., Valecillos, J., Izaddoust, S., Aguayo, A. T., Bilbao, J. "Coke deactivation and regeneration of HZSM-5 zeolite catalysts in the oligomerization of 1-butene", Applied Catalysis B: Environmental, 291, Article number: 120076, 2021. https://doi.org/10.1016/j.apcatb.2021.120076
[8] Muraza, O. "Maximizing Diesel Production through Oligomerization: A Landmark Opportunity for Zeolite Research", Industrial and Engineering Chemistry Research, 54(3), pp. 781–789, 2015. https://doi.org/10.1021/ie5041226
[9] Kriván, E., Tomasek, Sz., Hancsók, J. "The oligomerization of high olefin containing hydrocarbon by-products to clean engine fuels", Journal of Cleaner Production, 136, pp. 81–88, 2016. https://doi.org/10.1016/j.jclepro.2016.06.020
[10] Akah, A., Al-Ghrami, M., Saeed, M., Siddiqui, M. A. B. "Reactivity of naphtha fractions for light olefins production", International Journal of Industrial Chemistry, 8(2), pp. 221–233, 2017. https://doi.org/10.1007/s40090-016-0106-8
[11] Bringué, R., Cadenas, M., Fité, C., Iborra, M., Cunill, F. "Study of the oligomerization of 1-octene catalyzed by macroreticular ion-exchange resins", Chemical Engineering Journal, 207–208, pp. 226–234, 2012. https://doi.org/10.1016/j.cej.2012.06.089
[12] Kwon, M.-H., Chae, H.-J., Park, M. B. "Oligomerization of 1-hexene over designed SBA-15 acid catalysts", Journal of Industrial Engineering Chemistry, 65, pp. 397–405, 2018. https://doi.org/10.1016/j.jiec.2018.05.012
[13] Liu, J., Ding, N., Ge, Y., Zhou, X., Wang, J. A., Li, C. "Dimerization of Isobutene in C4 Mixtures in the Presence of Ethanol Over Acid Ion-Exchange Resin DH-2", Catalysis Letters, 149(5), pp. 1277–1285, 2019. https://doi.org/10.1007/s10562-019-02685-y
[14] Antunes, B. M., Rodrigues, A. E., Lin, Z., I. Portugal, I., Silva, C. M. "Alkenes oligomerization with resin catalysts", Fuel Processing Technology, 138, pp. 86–99, 2015. https://doi.org/10.1016/j.fuproc.2015.04.031
[15] Ying, L., Zhu, J., Cheng, Y., Wang, L., Li, X. "Kinetic modeling of C_2–C_7 olefins interconversion over ZSM-5 catalyst", Journal of Industrial Engineering Chemistry, 33, pp. 80–90, 2016. https://doi.org/10.1016/j.jiec.2015.09.021
[16] Huang, X., Aihemaitijiang, D., Xiao, W.-D. "Reaction pathway and kinetics of C_3–C_7 olefin transformation over high-silicon HZSM-5 zeolite at 400–490 °C", Chemical Engineering Journal, 280, pp. 222–232, 2015. https://doi.org/10.1016/j.cej.2015.05.124
[17] Kamal, S., Mahajani, S. "Kinetic study for oligomerization of acetaldehyde over cation exchange resin", Applied Catalysis A: General, 608, Article number: 117841, 2020. https://doi.org/10.1016/j.apcata.2020.117841
[18] Quann, R. J., Jaffe, S. B. "Structure-oriented lumping: describing the chemistry of complex hydrocarbon mixtures", Industrial and Engineering Chemistry Research, 31(11), pp. 2483–2497, 1992. https://doi.org/10.1021/ie00011a013
[19] Shahrouzi, J. R., Guillaume, D., Rouchon, P., Da Costa, P. "Stochastic Simulation and Single Events Kinetic Modeling: Application to Olefin Oligomerization", Industrial and Engineering Chemistry Research, 47(13), pp. 4308–4316, 2008. https://doi.org/10.1021/ie0712151

[20] Guillaume, D. "Network Generation of Oligomerization Reactions: Principles", Industrial and Engineering Chemistry Research, 45(13), pp. 4554–4557, 2006.
https://doi.org/10.1021/ie0510019

[21] Jin, F., Fan, Y., Yuan, M., Min, F., Wu, G., Ding, Y., Froment, G. F. "Single-event kinetic modeling of ethene oligomerization on ZSM-5", Catalysis Today, 316, pp. 129–141, 2018.
https://doi.org/10.1016/j.cattod.2018.05.020

[22] Jin, F., Zhang, P., Wu, G. "Fundamental kinetics model of acidity-activity relation for ethylene oligomerization and aromatization over ZSM-5 zeolites", Chemical Engineering Science, 229, Article number: 116144, 2021.
https://doi.org/10.1016/j.ces.2020.116144

[23] Izquierdo, J. F., Vila, M., Tejero, J., Cunill, F., Iborra, M. "Kinetic study of isobutene dimerization catalyzed by a macroporous sulphonic acid resin", Applied Catalysis A: General, 106(1), pp. 155–165, 1993.
https://doi.org/10.1016/0926-860X(93)80162-J

[24] Ebadzadeh, E., Khademi, M. H., Beheshti, M. "A kinetic model for methanol-to-propylene process in the presence of co-feeding of C_4-C_5 olefin mixture over H-ZSM-5 catalyst", Chemical Engineering Journal, 405, Articel number: 126605, 2021.
https://doi.org/10.1016/j.cej.2020.126605

[25] Ding, X., Geng, S., Li, C., Yang, C., Wang, G. "Effect of acid density of HZSM-5 on the oligomerization of ethylene in FCC dry gas", Journal of Natural Gas Chemistry, 18(2), pp. 156–160, 2009.
https://doi.org/10.1016/S1003-9953(08)60100-0

[26] Granollers, M., Izquierdo, J. F., Cunill, F. "Effect of macroreticular acidic ion-exchange resins on 2-methyl-1-butene and 2-methyl-2-butene mixture oligomerization", Applied Catalysis A: General, 435–436, pp. 163–171, 2012.
https://doi.org/10.1016/j.apcata.2012.05.051

[27] Gee, J. C., Williams, S. T. "Dimerization of linear olefins on Amberlyst® 15: Effects of chain length and double-bond position", Journal of Catalysis, 303, pp. 1–8, 2013.
https://doi.org/10.1016/j.jcat.2013.03.017

[28] Quann, R. J., Green, L. A., Tabak, S. A., Krambeck, F. J. "Chemistry of olefin oligomerization over ZSM-5 catalyst", Industrial and Engineering Chemistry Research, 27(4), pp. 565–570, 1988.
https://doi.org/10.1021/ie00076a006

[29] Guilera, J., Ramírez, E.,Fité, C., Iborra, M., Tejero, J. "Thermal stability and water effect on ion-exchange resins in ethyl octyl ether production at high temperature", Applied Catalysis A: General, 467, pp. 301–309, 2013.
https://doi.org/10.1016/j.apcata.2013.07.024

[30] Harmer, M. A., Sun, Q. "Solid acid catalysis using ion-exchange resins", Applied Catalysis A: General, 221(1–2), pp. 45–62, 2001.
https://doi.org/10.1016/S0926-860X(01)00794-3

[31] Bellussi, G., Mizia, F., Calemma, V., Pollesel, P., Millini, R. "Oligomerization of olefins from Light Cracking Naphtha over zeolite-based catalyst for the production of high quality diesel fuel", Microporous and Mesoporous Materials, 164, pp. 127–134, 2012.
https://doi.org/10.1016/j.micromeso.2012.07.020